Nonlinear analysis of circular double-skin concrete-filled steel tubular columns under axial compression

Liang, Q. Q. (2017). Nonlinear analysis of circular double-skin concrete-filled steel tubular columns under axial compression. *Engineering Structures*, 131: 639-650.

Nonlinear analysis of circular double-skin concrete-filled steel tubular columns under axial compression

Qing Quan Liang *

College of Engineering and Science, Victoria University, PO Box 14428, Melbourne, VIC 8001, Australia

Founder and President, Australian Association for Steel-Concrete Composite Structures (AASCCS), Melbourne, Australia

ABSTRACT

The use of the circular hollow steel tube in a circular concrete-filled steel tubular (CFST) column significantly alters the confinement mechanism in the conventional CFST column. The confinement models proposed for conventional circular CFST columns are therefore not applicable to circular double-skin CFST (DCFST) columns. This paper presents a new numerical model for predicting the structural performance of circular DCFST short columns under axial compression. The numerical model incorporates new material constitutive relationships of sandwiched concrete in circular DCFST columns. The confinement effects provided by the outer and inner steel tubes on the sandwiched concrete in circular DCFST columns are taken into account in the numerical formulations. Comparisons with existing experimental results on circular DCFST short columns are made to verify the numerical model developed. The numerical model is used to undertake parametric studies to examine the effects of important geometric and material parameters on the strength and ductility of axially loaded DCFST short columns. It is demonstrated that the numerical model can accurately capture the complete axial load-strain characteristics of circular DCFST short columns under axial compression. A design formula is proposed and found to predict well the ultimate axial loads of circular DCFST short columns.

* Corresponding author. Tel.: +61 3 9919 4134.
E-mail address: Qing.Liang@vu.edu.au (Q. Q. Liang)

Keywords: Concrete-filled steel tubes; Composite columns; Double-skin; Numerical modeling; Nonlinear analysis

1. Introduction

A circular double-skin concrete-filled steel tubular (DCFST) column is constructed by filling concrete between two concentric circular steel tubes as depicted in Fig. 1. This type of composite columns is recognized as a new form of double-skin composite panels used in submerged tube tunnels as studied by Wright et al. [1, 2] and Liang et al. [3, 4]. The use of the inner hollow steel tube in a CFST column not only remarkably reduces the structural weight but also significantly increases the bending stiffness, ductility and seismic performance of the CFST column. In addition, building services can be placed in the inner hollow steel tubes in DCFST columns. However, the use of the circular hollow steel tube in a circular CFST column obviously alters the confinement mechanism in the conventional CFST column. Consequently, the behavior of circular DCFST columns is significantly different from that of conventional circular CFST columns. This highlights the need for experimental studies on this type of composite columns. Extensive experimental studies on the structural performance of conventional circular CFST columns have been conducted in the past few decades [5-14]. However, experimental studies on the performance of circular DCFST short columns under axial compression are very limited [15-19].

Wei et al. [15] tested twenty-six circular double-skin steel tubular short columns filled with polymer concrete under axial compression to study the local instability issue and the strength and ductility enhancement due to the interaction. It was observed that the typical failure modes of DCFST short columns were the local buckling of the outer and inner steel tubes and

concrete shear failure in the buckled region. In addition, the DCFST short columns had the ultimate axial strengths of 10-30% higher than the sum of the strength of steel and concrete components. Moreover, the axial strain at the column ultimate load was much larger than the peak point strains of individual components. The test observations demonstrated that the confinement effect increased the strength and ductility of circular DCFST columns.

Experimental investigations into the behavior of six cold-formed circular DCFST short columns under axial compression were undertaken by Zhao et al. [16]. The diameter-to-thickness (D_o / t_o) ratios of the outer steel tubes ranged from 19 to 57 while the diameter-to-thickness (D_i / t_i) ratios of the inner steel tubes varied from 17 to 33. The sandwich between the two steel tubes was filled with concrete with average compressive cylinder strength of 63.4 MPa. However, the ends of all specimens were not strengthened by stiffeners to prevent the ends of the steel tubes from the premature failure. Two typical failure modes were observed, namely the so-called "elephant foot buckling" formed near the ends and the concrete diagonal shear failure. DCFST columns with slender outer steel sections were found to have higher ductility and energy absorption capacity than the hollow outer steel sections.

Tao at al. [17] conducted experiments to investigate the effects of the diameter (D_i / D_o) ratio of the inner-to-outer steel tubes and the diameter-to-thickness ratios of both steel tubes on the behavior of circular DCFST short columns. Twelve cold-formed circular DCFST short columns under axial compression were tested to failure. The D_i / D_o ratio of these tested specimens ranged from 0.267 to 0.778. The D_o / t_o ratios of the outer tubes ranged from 38 to 100 while the inner tubes had D_i / t_i ratios varying from 16 to 55. Test results showed that the outer steel tubes buckled locally outward while the inner steel tubes could buckle locally

inward depending on the D/t ratios of the tubes. Further tests on DCFST short columns under axial loading were conducted by Uenaka et al. [18]. They observed that the confinement effect existed in circular DCFST columns.

The behavior of conventional circular CFST columns has been studied analytically and numerically by researchers [7, 9, 10, 20-36]. Kostic et al. [37] developed a concentrated plasticity beam-column model based on the generalized plasticity material model for CFST beam-columns. The axial force and bending moment interaction, gradual yielding and strain hardening of material and nonlinear geometry under large displacements were taken into account in the model. The proposed model was shown to be accurate and computationally efficient. However, there are very few numerical models developed for simulating the performance of circular DCFST short columns [17, 38-41]. The analytical model proposed by Wei et al. [38] for double-skin polymer concrete-filled steel tubular columns considered the confinement effect. The material stress-strain relationships of confined polymer concrete were a function of the effective lateral confining stress, which was determined by using an iterative procedure. Tao et al. [17] developed a fiber element model for the nonlinear analysis of axially loaded circular DCFST columns. The material constitutive model for confined concrete in conventional circular CFST columns was used in the analysis of circular DCFST columns and the effect of the inner steel tube on the concrete confinement was not considered. They recognized that the fiber element model needs to be improved in order to accurately predict the post-peak behavior of DCFST short columns. The commercial finite element program ABAQUS was used by Huang et al. [39] to simulate the responses of DCFST short columns under axial loading. The stress-strain relationship for confined concrete in conventional circular CFST columns given by Han et al. [42] was used to model the material behavior of sandwiched concrete in circular DCFST columns.

Hu and Su [40] proposed three lateral confining pressure models based on experimental results presented by Tao et al. [17] and finite element analysis results for confined concrete in circular DCFST columns. In these models, the lateral confining pressure was expressed as a function of the geometric parameters of the outer and inner steel tubes or combined geometric parameters and yield strength of steel tubes. A material degradation factor was also proposed for modeling the post-peak behavior of the confined concrete. The proposed model and material degradation factor were used in the stress-strain relationship for sandwiched concrete in DCFST short columns. The models proposed by Hu and Su [40] were employed by Pagoulatou et al. [41] in the finite element models developed for the nonlinear analysis of DCFST short columns under axial loading. The results showed that the confining pressure models by Hu and Su generally yielded more accurate predictions of the structural performance of DCFST columns than the ones for concrete in conventional CFST columns.

It should be noted that the confinement model proposed by Hu and Su [40] was based on limited test data. Further evaluations of their lateral confining pressure models are necessary. Moreover, new models need to be developed to accurately determine the post-peak behavior of the sandwiched concrete confined by the outer and inner steel tubes. This paper presents accurate constitutive models developed based on the previous work for simulating the material behavior of confined concrete in circular DCFST columns. The new material constitutive relationships are incorporated in the numerical model based on the fiber element formulation to predict the behavior of DCFST short columns under axial compression. The accuracy of the lateral confining pressure models given by Hu and Su [40] is examined. The numerical model is used to investigate the effects of various geometric and material parameters on the strength and ductility of circular DCFST short columns. A design model is proposed for the design of circular DCFST short columns.

2. The numerical model

2.1. General

There are three numerical models that can be used to undertake the nonlinear inelastic analysis of composite columns, including the continuum finite element model, fiber element model and inelastic beam-column model [37, 43-46]. In the finite element modeling, the column is divided into three dimensional elements with many degrees of freedom along its length. In addition, contract elements need to be used to model the interaction between the steel tubes and the sandwiched concrete. Because there are many degrees of freedom in a finite element model, the computational cost of the nonlinear finite element analysis is very high compared to the fiber element model, where the discretization of the column along its length is not required. In this paper, therefore, the numerical model is formulated based on the fiber element method. The typical fiber element discretization of the cross-section of the circular DCFST column is illustrated in Fig. 2. The outer steel tube, the inner steel tube and the sandwiched concrete can be assigned different material properties. The material uniaxial stress-strain relationships are used to calculate fiber stresses from fiber strains. The axial force acting on the cross-section is determined as the stress resultant.

2.2. Stress-strain relationships for sandwiched concrete

The confinement mechanism in circular DCFST short columns is different from that in conventional circular CFST short columns [18, 46]. When the expansion of the concrete in a circular DCFST column exceeds that of the steel tubes, radial pressures develop at the interfaces between the outer steel tube, the sandwiched concrete and the inner steel tube. The

outer steel tube is in hoop tension while the inner steel tube is under hoop compression. The sandwiched concrete is subjected to triaxial stresses, the outer steel tube is under biaxial stresses and the inner steel tube is in biaxial compression. It is noted that both the outer and inner steel tubes provide confinement to the sandwiched concrete. However, the yield stress of the steel tubes in the longitudinal direction is reduced by the presence of the hoop tension or hoop compression.

The idealized stress-strain curve depicted in Fig. 3 is used to simulate the material behavior of the sandwiched concrete in circular DCFST columns. The stress-strain curve consists of three parts: the ascending part OA, the linearly descending part AB and the constant part BC. The material laws for confined concrete given by Mander et al. [47] are adopted here to model the part OA of the stress-strain curve, which is expressed by

$$\sigma_c = \frac{f_{cc}^{'}\lambda\left(\varepsilon_c/\varepsilon_{cc}^{'}\right)}{\lambda-1+\left(\varepsilon_c/\varepsilon_{cc}^{'}\right)^{\lambda}} \tag{1}$$

$$\lambda = \frac{E_c}{E_c-\left(f_{cc}^{'}/\varepsilon_{cc}^{'}\right)} \tag{2}$$

in which σ_c denotes the longitudinal compressive stress of concrete, $f_{cc}^{'}$ is the compressive strength of the confined concrete, ε_c stands for the longitudinal compressive strain of concrete, $\varepsilon_{cc}^{'}$ is the strain at $f_{cc}^{'}$ and E_c is the Young's modulus of concrete. The Young's modulus of concrete can be calculated by the following formula given in ACI-318 [48]:

$$E_c = 3320\sqrt{\gamma_c f_c^{'}} + 6900 \text{ (MPa)} \tag{3}$$

where γ_c is the strength reduction factor, which is used to take into account the effects of the column size on the compressive strength of concrete in real columns [43, 44]. For the sandwiched concrete in circular DCFST columns, the strength reduction factor γ_c proposed by Liang [43, 44] is modified as follows:

$$\gamma_c = 1.85 t_c^{-0.135} \quad (0.85 \le \gamma_c \le 1.0) \tag{4}$$

in which t_c is the thickness of the sandwiched concrete and is taken as $t_c = D_o/2 - t_o - D_i/2$, where D_o and t_o are the diameter and thickness of the outer steel tube respectively and D_i is the diameter of the inner steel tube.

The compressive strength $f_{cc}^{'}$ and corresponding strain $\varepsilon_{cc}^{'}$ of the sandwiched concrete in the circular DCFST column is a function of the lateral confining pressure (f_{rp}) exerted by the outer and inner steel tubes. The confinement model given by Mander et al. [47] for reinforced concrete has commonly been used to determine the compressive strength and strain of the confined concrete in CFST columns [31, 32]. This confinement model is implemented in the present numerical model with the strength reduction factor γ_c:

$$f_{cc}^{'} = \gamma_c f_c^{'} + k_1 f_{rp} \tag{5}$$

$$\varepsilon_{cc}^{'} = \varepsilon_c^{'}\left(1 + k_2 \frac{f_{rp}}{\gamma_c f_c^{'}}\right) \tag{6}$$

where $k_1 = 4.1$ and $k_2 = 20.5$ according to the experiment study conducted by Richart et al. [49]. The strain $\varepsilon_c^{'}$ corresponding to $f_c^{'}$ of the unconfined concrete depends on the effective compressive strength ($\gamma_c f_c^{'}$) of concrete, which is determined by [43]:

$$\varepsilon_c^{'} = \begin{cases} 0.002 & \text{for } \gamma_c f_c^{'} \le 28\,(\text{MPa}) \\ 0.002 + \dfrac{\gamma_c f_c^{'} - 28}{54000} & \text{for } 28 < \gamma_c f_c^{'} \le 82\,(\text{MPa}) \\ 0.003 & \text{for } \gamma_c f_c^{'} > 82\,(\text{MPa}) \end{cases} \tag{7}$$

The lateral confining pressure depends on the geometric and material properties of the cross-sections of circular CFST columns. Liang and Fragomeni [28] proposed lateral confining pressure models for concrete in conventional circular CFST columns. However, the confinement mechanism in circular DCFST columns is different from that in conventional circular CFST columns as discussed previously. Therefore, new models accounting for the effects of the inner steel tube need to be developed for the sandwiched concrete. Based on test results reported by Tao et al. [17], Hu and Su [40] developed the following three lateral confining pressure models for sandwiched concrete in circular DCFST columns:

$$f_{rp} = 8.525 - 0.166\left(\frac{D_o}{t_o}\right) - 0.00897\left(\frac{D_i}{t_i}\right) + 0.00125\left(\frac{D_o}{t_o}\right)^2 + 0.00246\left(\frac{D_o}{t_o}\right)\left(\frac{D_i}{t_i}\right) - 0.0055\left(\frac{D_i}{t_i}\right)^2 \ge 0 \tag{8}$$

$$\frac{f_{rp}}{f_{syi}} = 0.01844 - 0.00055\left(\frac{D_o}{t_o}\right) + 0.0004\left(\frac{D_i}{t_i}\right) + 0.00001\left(\frac{D_o}{t_o}\right)^2 + 0.00001\left(\frac{D_o}{t_o}\right)\left(\frac{D_i}{t_i}\right) - 0.00002\left(\frac{D_i}{t_i}\right)^2 \tag{9}$$

$$\frac{f_{rp}}{f_{syo}} = 0.01791 - 0.00036\left(\frac{D_o}{t_o}\right) - 0.00013\left(\frac{D_i}{t_i}\right) + 0.00001\left(\frac{D_o}{t_o}\right)^2 + 0.00001\left(\frac{D_o}{t_o}\right)\left(\frac{D_i}{t_i}\right) - 0.00002\times\left(\frac{D_i}{t_i}\right)^2 \geq 0 \tag{10}$$

where D_i, t_i and f_{syi} are the diameter, thickness and yield strength of the inner steel tube, respectively and f_{syo} is the yield strength of the outer steel tube.

It should be noted that Eqs. (8)-(10) were proposed based on the results of limited tests on circular DCFST short columns with $20 \leq D_o / t_o \leq 100$ and $15 \leq D_i / t_i \leq 55$ [17, 40]. The validation presented in Section 4 demonstrate that Eqs. (9) and (10) significantly overestimate the lateral confining pressures on the sandwiched concrete in DCFST columns. It is suggested that Eqs. (9) and (10) should not be used. Eq. (8) is therefore implemented in the fiber element model to compute the lateral confining pressures on the sandwiched concrete. It should be noted that when $D_i / t_i = 0$, the column becomes a conventional CFST column. The constitutive model proposed for sandwiched concrete should give reasonable predictions of the behavior of conventional CFST columns. However, more accurate stress-strain relationships for confined concrete proposed by Liang and Fragomeni [28] should be used to simulate the behavior of conventional CFST columns.

The parts *AB* and *BC* of the stress-strain curve presented in Fig. 3 can be expressed by

$$\sigma_c = \begin{cases} \beta_c f_{cc}^{'} + \left(\dfrac{\varepsilon_{cu} - \varepsilon_c}{\varepsilon_{cu} - \varepsilon_{cc}^{'}}\right)\left(f_{cc}^{'} - \beta_c f_{cc}^{'}\right) & \text{for } \varepsilon_{cc}^{'} < \varepsilon_c \leq \varepsilon_{cu} \\ \beta_c f_{cc}^{'} & \text{for } \varepsilon_c > \varepsilon_{cu} \end{cases} \tag{11}$$

In the present study, the strain ε_{cu} and factor β_c are used to determine the post-peak behavior of the sandwiched concrete in DCFST columns. The strain ε_{cu} and factor β_c reflect the confinement effect provided by the outer and inner steel tubes on the sandwiched concrete. Based on the test results reported by Tao et al. [17], the strain ε_{cu} is proposed as follows:

$$\varepsilon_{cu} = \begin{cases} 0.03 & \text{for } D_o/t_o \le 60 \\ 0.023 + (100 - D_o/t_o)(0.03 - 0.023)/(100 - 60) & \text{for } 60 < D_o/t_o \le 100 \\ 0.02 & \text{for } D_o/t_o > 100 \end{cases} \tag{12}$$

It is seen from above equation that for $60 < D_o/t_o \le 100$, the strain ε_{cu} is between 0.023 and 0.03 and is determined by the linear interpolation.

A strength degradation parameter k_3 was proposed by Hu and Su [40] to model the post-peak behavior of the sandwiched concrete as follows:

$$k_3 = 1.73916 - 0.00862\left(\frac{D_o}{t_o}\right) - 0.04731\left(\frac{D_i}{t_i}\right) - 0.00036\left(\frac{D_o}{t_o}\right)^2 + 0.00134\left(\frac{D_o}{t_o}\right)\left(\frac{D_i}{t_i}\right) - 0.00058\left(\frac{D_i}{t_i}\right)^2 \ge 0 \tag{13}$$

However, it has been found that k_3 calculated using Eq. (13) could be negative, zero or greater than 1.0 for some cross-sections as shown in Table 1. For example, when $D_o/t_o = 30$ and $D_i/t_i < 12$, k_3 is greater than 1.0. Eq. (13) is therefore not used alone to determine the strength degradation of concrete rather it is incorporated in the following expressions for β_c $(0 \le \beta_c \le 1.0)$ proposed here for the sandwiched concrete in circular DCFST columns:

$$\beta_c = \begin{cases} 1.0 & \text{for } D_o/t_o \le 40 \\ k_3 & \text{for } D_o/t_o > 40 \\ 0.0000339(D_o/t_o)^2 - 0.010085(D_o/t_o) + 1.349 & \text{for } k_3 < 0 \end{cases} \quad (14)$$

It can be seen from above expression that when $D_o/t_o \le 40$, the outer steel tube provides significant confinement to the sandwiched concrete so that β_c is taken as 1.0 as suggested by Liang [31, 32]. In addition, when $k_3 < 0$, the formula given by Hu et al. [23] is used in Eq. (14) to calculate β_c, which depends on the D_o/t_o ratio of the outer steel tube. The factor β_c for the case of $D_o/t_o \le 40$ or $k_3 < 0$ is proposed based on the assumption that the inner steel tube does not buckle locally so that it can provide confinement to the sandwiched concrete in DCFST columns. It should be noted that the strength degradation parameter k_3 is within the range of $0 \le k_3 \le 1.0$.

2.3. Stress-strain relationships for structural steels

As discussed in the preceding section, both the outer and inner steel tubes of the circular DCFST short column under axial compression are subjected to biaxial stresses because of the confinement effect. The yield stress in the longitudinal direction is reduced by the presence of hoop tension in the outer steel tube or hoop compression in the inner steel tube. The confinement effect on the steel yield strength is considered in the idealized linear-rounded-linear stress-strain curve for structural steels illustrated in Fig. 4. For high-strength steels, a straight line is used to replace the rounded part of the stress-strain curve. The expression for the rounded part of the stress-strain curve was given by Liang [43].

2.4. Strain ductility index

The axial ductility of a DCFST column under axial compression is evaluated by the strain ductility index, which is expressed by

$$PI_{sd} = \frac{\varepsilon_u}{\varepsilon_y} \tag{17}$$

where ε_u represents the axial strain of the DCFST short column corresponding to the axial load which is 90% of its ultimate axial strength in the post-peak range. If the column exhibits an ascending post-yield behavior, ε_u is taken as the ultimate axial strain. The yield strain ε_y of the short column is calculated as $\varepsilon_{0.75}/0.75$, where $\varepsilon_{0.75}$ denotes the axial strain corresponding to the axial load which attains 75% of its ultimate axial strength in the pre-peak range [17, 28, 50].

3. Verification of the numerical model

The ultimate axial strengths of DCFST short columns predicted by the computer program are compared with experimental results reported by Tao et al. [17] and Uenaka et al. [18]. The geometric and material properties of tested specimens are provided in Table 2. Circular DCFST columns tested by Tao et al. [17] had D_i/D_o ratios ranging from 0.267 to 0.778, D_o/t_o ratios ranging from 38 to 100 and D_i/t_i ratios ranging from 16 to 55. The compressive strength of concrete cylinder ($f_c^{'}$) was taken as 0.85 times that of the concrete cube. It is noted that the lateral confining pressure model adopted in the present numerical model is applicable only to DCFST columns with $20 \le D_o/t_o \le 100$ and $15 \le D_i/t_i \le 55$. Therefore,

only those specimens tested by Uenaka [18] within the ranges of $20 \le D_o / t_o \le 100$ and $15 \le D_i / t_i \le 55$ were selected for comparison purpose. The tensile strength of all steel tubes was assumed to be 430 MPa in the analyses.

The ultimate axial strengths of circular DCFST short columns predicted by the numerical analysis ($P_{u.\mathrm{num}}$) and experimental ultimate axial strengths ($P_{u.\mathrm{exp}}$) are listed in Table 2. It can be seen from Table 2 that there is a good agreement between computational solutions and experimental measurements. The mean ratio of the predicted ultimate axial strength to the measured value of the tested specimens is 0.99. The statistical analysis conducted shows that the standard deviation of $P_{u.\mathrm{num}} / P_{u.\mathrm{exp}}$ is 0.060 with a coefficient of variation of 0.061, which is within the acceptable range of 10%.

The predicted axial load-strain curves for Specimens cc2a, cc3a, cc5a and cc7a are compared against experimental results provided by Tao et al. [17] in Fig. 5. The figure shows that the computer program predicts well the experimentally observed axial load-strain behavior of DCFST short columns. The post-peak behavior of Specimens cc2a, cc3a and cc7a with D_o / t_o ratios ranging from 60 to 100 is characterized by the descending stress-strain curves. However, due to its small D_o / t_o ratio of 38, the Specimen cc5a experienced strain-hardening behavior in the post-yield range. It appears that the predicted post-yield behavior of DCFST columns is in excellent agreement with corresponding test data. This implies that the proposed strain ε_{cu} and factor β_c can accurately determine the post-yield behavior of circular DCFST columns. However, there is a slight difference between the computational and experimental initial axial stiffness as depicted in Fig. 5. This may be caused by the uncertainty of the

concrete strength and stuffiness. It can be concluded that the numerical model can accurately capture the complete axial load-strain characteristics of circular DCFST short columns.

4. Validation of lateral confining pressure models

The lateral confining pressure model plays an important role in determining the stress-strain behavior of the sandwiched concrete in circular DCFST columns. The lateral confining pressure models proposed by Hu and Su [40] have been implemented in the computer program and their accuracy is examined in this section. The lateral confining pressures (f_{rp}) and ultimate axial strengths (P_u) of 15 tested DCFST short columns predicted by three models and the computer program are given in Table 3, where the subscripts 1, 2 and 3 represent the confining pressure or the ultimate axial strength computed using Eqs. (8), (9) and (10) respectively. The geometric and material properties of these specimens can be found in Table 2. It can be seen from Table 3 that Eq. (8) yields good predictions of the lateral confining pressures on the sandwiched concrete, which leads to the accurate estimations of the ultimate axial strengths of DCFST columns. However, Eqs (9) and (10) significantly overestimate the lateral confining pressures on the sandwiched concrete. As a result, the mean ultimate axial strength of these columns calculated based on Eqs. (9) and (10) is overestimated by 60.2% and 43.3% respectively. Therefore, it is suggested that Eq. (8) should be used in numerical models to determine the lateral confining pressures on the sandwiched concrete in circular DCFST columns and Eqs. (9) and (10) should not be used.

5. Parametric study

The parametric study was conducted to investigate the effects of the D_i / D_o ratio, D_o / t_o ratio, D_i / t_i ratio, concrete compressive strength and steel yield strength on the structural performance of circular DCFST short columns. Six groups of full-scale size circular DCFST columns with various geometric and material parameters were analyzed by the computer program developed. The geometric and material properties of these columns are given in Table 4. The same material properties were specified for the outer and inner steel tubes in a DCFST column. The Young's modulus of steel tubes was taken as 200 GPa.

5.1. Effects of D_i / D_o ratio

The D_i / D_o ratio of the inner and outer steel tubes is an important parameter that influences the structural performance of DCFST short columns. The D_i / D_o ratios of 0.3, 0.4, 0.5, 0.6 and 0.7 were determined by varying the diameter of the inner steel tube but keeping its thickness unchanged as shown in Group 1 in Table 4. It can be seen from Table 4 that increasing the D_i / D_o ratio or D_i / t_i ratio decreases the lateral confining pressure on the sandwiched concrete. When $D_i / t_i \geq 40$, the lateral confining pressure is zero. The axial load-strain curves for DCFST short columns with various D_i / D_o ratios are presented in Fig. 6. It can be observed from Fig. 6 that the D_i / D_o ratio has an insignificant effect on the initial axial stiffness of DCFST short columns. In addition, increasing the D_i / D_o ratio from 0.3 to 0.4, 0.5, 0.6 and 0.7 reduces the ultimate axial strength of the DCFST short column by 4.8%, 12.5%, 22.7% and 26.9%, respectively. This is because the cross-sectional area of the sandwiched concrete is reduced significantly but the cross-sectional area of the inner steel tube is increased considerably. Moreover, the slope of the post-peak stress-strain curve is found to decrease with an increase in the D_i / D_o ratio. As demonstrated in Fig.7, the axial

ductility of DCFST short columns increases with increasing the D_i/D_o ratio. The strain ductility indices of the DCFST columns with the D_i/D_o ratios of 0.3, 0.4, 0.5, 0.6 and 0.7 are 5.78, 6.47, 7.38, 9.74 and 10.36, respectively. This can be explained by the fact that increasing the D_i/D_o ratio of the DCFST column decreases the concrete area but increases the steel area. As a result, the axial ductility of the column is shown to improve.

5.2. Effects of D_o/t_o ratio

Two cases were considered to examine the effects of D_o/t_o ratio on the performance of DCFST columns. The first case was to vary the diameter of the outer steel tubes while keeping their thickness unchanged as shown in Group 2 in Table 4. As demonstrated in Table 4, the lateral confining pressure increases with increasing the D_o/t_o ratio. Fig. 8 presents the axial load-strain curves for DCFST columns with various D_o/t_o ratios. The initial axial stiffness of DCFST short column is considerably increased by increasing the D_o/t_o ratio. It appears that increasing the D_o/t_o ratio significantly increases the ultimate axial strength of DCFST short columns with the same D_i/t_i ratio. When the D_o/t_o ratio is increased from 50 to 55, 60, 65 and 70, the column ultimate axial load is found to increase by 18.5%, 39.1%, 62% and 87.6%, respectively. As demonstrated in Fig. 8, the D_o/t_o ratio has a remarkable effect on the post-peak behavior of DCFST columns. The effects of D_o/t_o ratio on the strain ductility index are illustrated in Fig. 9. It can be seen that increasing the D_o/t_o ratio significantly reduces the strain ductility index. The strain ductility index is reduced from 9.25 to 7.41, 6.16, 5.2 and 4.55 by increasing the D_o/t_o ratio from 50 to 55, 60, 65 and 70, respectively.

As illustrated in Group 3 in Table 4, the second case was to keep the diameter $D_o = 600\,\text{mm}$ of the outer steel tube unchanged but to vary the thickness of the outer steel tube to give D_o/t_o ratios of 50, 55, 60, 65 and 70. It can be observed from Table 4 that the lateral confining pressure increases with an increase in the D_o/t_o ratio regardless of the diameter of the outer steel tube. It can be observed from Fig. 10 that increasing the D_o/t_o ratio decreases the initial axial stiffness and remarkably reduces the post-peak axial stiffness. The ultimate axial load of DCFST short column is slightly reduced by increasing the D_o/t_o ratio. This suggests that increasing the diameter of the outer steel tube is more effective in increasing the ultimate axial load of the DCFST column than increasing the thickness of the outer steel tube when keep the same D_o/t_o ratio and other conditions. As shown in Fig.11, increasing the D_o/t_o ratio leads to a remarkable decrease in the strain ductility of DCFST columns. For DCFST columns with D_o/t_o ratios of 50, 55, 60, 65 and 70, the corresponding strain ductility indices are 8.37, 7.14, 6.16, 5.31 and 4.69, respectively.

5.3. Effects of D_i/t_i ratio

In Group 4, the D_i/t_i ratios of 25, 30, 35, 40 and 45 were computed by changing the thickness of the inner steel tube. It appears from Table 4 that increasing the D_i/t_i ratio decreases the lateral confining pressure. Fig. 12 presents the axial load-strain curves for circular DCFST columns with various D_i/t_i ratios. It can be observed from Fig. 12 that the D_i/t_i ratio has neglectable effect on the initial axial stiffness of the DCFST short columns. In addition, three DCFST columns under consideration exhibit strain softening behavior in the post-yield range owing to the large D_o/t_o ratio of 55. Moreover, the numerical results show

that increasing the D_i/t_i ratio significantly decreases the ultimate axial load of DCFST columns. The effects of D_i/t_i ratio on the strain ductility index are illustrated in Fig. 13. When increasing the D_i/t_i ratio from 25 to 35, the strain ductility index increases slightly from 5.82 to 6.05. However, when increasing the D_i/t_i ratio from 35 to 45, the strain ductility index decreases from 6.05 to 5.21.

5.4. Effects of concrete compressive strength

DCFST short columns in Group 5 were filled with concrete of different strengths. In the numerical analyses, the compressive cylinder strength of the sandwiched concrete was taken as 40, 55, 70, 85 and 100 MPa respectively. It is interesting to note that the lateral confining pressure is not affected by the concrete compressive strength. The predicted axial load-strain curves for DCFST short columns with various concrete strengths are given in Fig. 14. The results show that increasing the concrete compressive strength considerably increases the initial axial stiffness of DCFST columns. The use of high-strength concrete results in a significant increase in the ultimate axial load of the DCFST short column. When increasing the concrete strength from 40 to 100 MPa, the column ultimate axial load is found to increase by 63.95%. This suggests that it is effective to use high-strength concrete to increase the ultimate axial strengths of DCFST short columns. Fig. 15 provides the strain ductility index as a function of the concrete compressive strength. It appears that the higher the concrete strength, the lower the strain ductility index. The DCFST column filled with normal strength concrete of 40 MPa has a strain ductility index of 5.25. However, it is only 3.32 when high strength concrete of 100 MPa is used because of the brittle nature of high-strength concrete.

5.5. Effects of steel yield strength

Circular DCFST short columns in Group 6 shown in Table 4 were analyzed to study the effects of steel yield strength on their strength and ductility. It can be seen from Table 4 that the steel yield strength does not affect the lateral confining pressure. The axial load-strain curves for circular DCFST columns with different steel yield strengths are shown in Fig. 16. The figure illustrates that the initial axial stiffness of DCFST short columns is not affected by the steel yield strength. However, increasing the steel yield strength significantly increases the ultimate axial load of the DCFST column. The column ultimate axial load is increased by 5.9%, 11.8%, 15.4% and 23.6% respectively by increasing the steel yield strength from 250 to 300, 350, 380 and 450 MPa. The strain ductility indices of these DCFST columns made of different strength steel tubes are given in Fig. 17. For DCFST columns with the steel yield strengths of 250 to 300, 350, 380 and 450 MPa, the strain ductility indices are 4.1, 4.34, 4.35, 4.31 and 4.07, respectively. This indicates that the yield strength of normal strength steel tubes does not have a significant effect on the strain ductility of DCFST short columns.

5.6 Load and stress distributions

The DCFST column C13 given in Table 4 was analyzed to investigate the axial load and longitudinal stress distributions within its cross-section. Fig. 18 depicts the axial loads carried by the inner steel tube, outer steel tube, sandwiched concrete and DCFST column as a function of the axial strain. It can be observed from the figure that the axial loads carried by the inner steel tube, the outer steel tube, the sandwiched concrete at the ultimate limit state are 10.38%, 26.63% and 62.99% of the ultimate axial load of the DCFST column, respectively. The sandwiched concrete carries a large portion of the ultimate axial load. The distribution of

the longitudinal stresses in the inner steel tube, the outer steel tube and the sandwiched concrete at different axial strain levels is presented in Fig. 19. When the axial strain is less than 0.006, the longitudinal stresses in steel and concrete components are found to increase with an increase in the axial strain. The DCFST column attains its ultimate axial strength at an axial strain of 0.006. It appears that the compressive stress of the sandwiched concrete at the axial strain of 0.006 is higher than $f_c^{'}$ due to the confinement effect. When increasing the axial strain greater than 0.006, the compressive stress in the sandwiched concrete decreases but the longitudinal stresses in both steel tubes are shown to increase due to strain hardening as illustrated in Fig. 19.

6. Proposed design model

The ultimate axial load of a circular DCFST short column is governed by its geometric and material properties. A design formula considering confinement effects was proposed by Liang and Fragomeni [28] for the design of conventional circular CFST short columns. The concept is adopted here to develop a simple model for design purpose. Based on numerical analyses and experimental results, a new design formula for calculating the ultimate axial load of circular DCFST short columns incorporating the confinement effect is proposed as

$$P_u = \left(\gamma_c f_c^{'} + 4.1 f_{rp}\right) A_c + \gamma_{so} f_{syo} A_{so} + \gamma_{si} f_{syi} A_{si} \tag{18}$$

where f_{rp} is calculated by using Eq. (8), A_c is the cross-sectional area of the sandwiched concrete, A_{so} is the cross-sectional area of the outer steel tube, and A_{si} is the cross-sectional area of the inner steel tube. The coefficients γ_{so} and γ_{si} are the strength factors for the outer and inner steel tubes respectively, which account for the effects of hoop stresses, strain

hardening, geometric imperfections and residual stresses. The strength factor γ_s proposed by Liang and Fragomeni [28] can be applied to both the outer and inner steel tubes as follows:

$$\gamma_{so} = 1.458\left(\frac{D_o}{t_o}\right)^{-0.1} \qquad (0.9 \le \gamma_{so} \le 1.1) \tag{19}$$

$$\gamma_{si} = 1.458\left(\frac{D_i}{t_i}\right)^{-0.1} \qquad (0.9 \le \gamma_{si} \le 1.1) \tag{20}$$

To examine the accuracy of the proposed design model, the ultimate axial loads of DCFST short columns calculated using Eq. (18) are compared against test data in Table 5, where $P_{u.\mathrm{cal}}$ is the ultimate axial load calculated using Eq. (18). The results given in Table 5 demonstrate that there is a good agreement between the calculated and experimental results. The mean of the calculated ultimate axial loads is 97.9% of that of the experimental values. The statistical analysis undertaken shows that the standard deviation of $P_{u.\mathrm{cal}}/P_{u.\exp}$ is 0.057 and its coefficient of variation is 0.058. This implies that the proposed design formula can be used in the design of circular DCFST short column under axial compression in practice.

7. Conclusions

This paper has presented a numerical model for simulating the behavior of circular double-skin concrete-filled steel tubular (DCFST) short columns under axial compression. The stress-strain relationships for the sandwiched concrete in circular DCFST columns, which recognizes the confinement effects provided by both the outer and inner steel tubes, have been proposed based on the previous work. The concrete strain and strength degradation factor have been proposed and shown to model well the post-peak behavior of DCFST columns.

Comparative studies have been undertaken to examine the accuracy of various lateral confining pressure models for sandwiched concrete in circular DCFST columns. The accurate lateral confining pressure model has been identified and implemented in the stress-strain relationships for the sandwiched concrete in circular DCFST columns. The accuracy of the numerical model developed has been verified by comparisons of computer solutions with experimentally observed behaviors of DCFST short columns reported by independent researchers. The developed material laws for sandwiched concrete can be implemented in nonlinear analysis techniques to simulate the behavior of DCFST columns. The results obtained in the parametric study on full-scale size DCFST short columns with various important geometric and material parameters can be used to validate other numerical models. The proposed design formula has been shown to yield accurate predictions of the ultimate axial loads of DCFST short columns and can be used in practice.

References

[1] Wright HD, Oduyemi TOS, Evans HR. The experimental behavior of double skin composite elements. Journal of Constructional Steel Research 1991; 19(2): 97-110.

[2] Wright HD, Oduyemi TOS, Evans HR. The design of double skin composite elements. Journal of Constructional Steel Research 1991; 19(2): 111-132.

[3] Liang QQ, Uy B, Wright HD, Bradford MA. Local and post-local buckling of double skin composite panels. Structures and Buildings, Proceedings of The Institution of Civil Engineers, UK 2003; 156(2): 111-119.

[4] Liang QQ, Uy B, Wright HD, Bradford MA. Local buckling of steel plates in double skin composite panels under biaxial compression and shear. Journal of Structural Engineering, ASCE 2004; 130(3): 443-451.

[5] Furlong RW. Strength of steel-encased concrete beam-columns. Journal of the Structural Division, ASCE 1967; 93(5): 113-124.

[6] Knowles RB, Park R. Strength of concrete-filled steel tubular columns. Journal of the Structural Division, ASCE 1969; 95(12):2565-2587.

[7] Neogi, PK, Sen HK, Chapman JC. Concrete-filled tubular steel columns under eccentric loading. The Structural Engineer 1969; 47(5): 187-195.

[8] Tomii M, Yoshimura K, Morishita Y. Experimental studies on concrete filled steel tubular stub columns under concentric loading. Proceedings of the International Colloquium on Stability of Structures under Static and Dynamic Loads, 1977, pp. 718-741.

[9] Rangan B, Joyce M. Strength of eccentrically loaded slender steel tubular columns filled with high-strength concrete. ACI Structural Journal 1992; 89(6): 676-681.

[10] Schneider SP. Axially loaded concrete-filled steel tubes. Journal of Structural Engineering, ASCE 1998; 124(10):1125-1138.

[11] O'Shea MD, Bridge RQ. Design of circular thin-walled concrete filled steel tubes. Journal of Structural Engineering, ASCE 2000; 126(11):1295-1303.

[12] Giakoumelis, G, Lam D. Axial load capacity of circular concrete-filled tube columns. Journal of Constructional Steel Research 2004; 60: 1049-1068.

[13] Sakino K, Nakahara H, Morino S, Nishiyama I. Behavior of centrally loaded concrete-filled steel-tube short columns. Journal of Structural Engineering, ASCE 2004; 130(2):180-188.

[14] Portolés JM, Romero, ML, Bonet JL, Filippou FC. Experimental study of high strength concrete-filled circular tubular columns under eccentric loading. Journal of Constructional Steel Research 2011; 67(4): 623-633.

[15] Wei S, Mau ST, Vipulanandan C, Mantrala SK. Performance of new sandwich tube under axial loading: Experiment. Journal of Structural Engineering, ASCE 1995; 121(12): 1806-1814.

[16] Zhao XL, Grzebieta R, Elchalakan M. Tests of concrete-filled double skin CHS composite stub columns. Steel and Composite Structures 2002; 2(2): 129-146.

[17] Tao Z, Han LH, Zhao XL. Behavior of concrete-filled double skin (CHS inner and CHS outer) steel tubular stub columns and beam-columns. Journal of Constructional Steel Research 2004; 60: 1129-1158.

[18] Uenaka K, Kitoh H, Sonoda K. Concrete filled double skin circular stub columns under compression. Thin-Walled Structures 2010; 48: 19-24.

[19] Han LH, Huang H, Tao Z, Zhao XL. Concrete-filled double skin steel tubular (CFDST) beam–columns subjected to cyclic bending**.** Engineering Structures 2006; 28(12):1698-1714.

[20] Hajjar JF, Schiller PH, Molodan A. A distributed plasticity model for concrete-filled steel tube beam-columns with interlayer slip. Eng Struct 1998;20(8):663-676.

[21] Susantha KAS, Ge HB, Usami T. Uniaxial stress-strain relationship of concrete confined by various shaped steel tubes. Eng Struct 2001;23(10):1331-1347.

[22] Shanmugam NE, Lakshmi B, Uy B. An analytical model for thin-walled steel box columns with concrete in-fill. Eng Struct 2002;24(6):825-838.

[23] Hu, HT, Huang CS, Wu MH, Wu YM. Nonlinear analysis of axially loaded concrete-filled tube columns with confinement effect. Journal of Structural Engineering, ASCE 2003; 129(10): 1322-1329.

[24] Gayathri V, Shanmugam NE, Choo YS. Concrete-filled tubular columns, Part 1−Cross-section analysis. International Journal of Structural Stability and Dynamics 2004; 4(4): 459-478.

[25] Hu HT, Huang CS, Chen ZL. Finite element analysis of CFT columns subjected to an axial compressive force and bending moment in combination. Journal of Constructional Steel Research 2005; 61(12): 1692-1712.

[26] Ellobody E, Young B, Lam D. Behaviour of normal and high strength concrete-filled compact steel tube circular stub columns. Journal of Constructional Steel Research 2006; 62: 706-715.

[27] Hatzigeorgiou GD. Numerical model for the behavior and capacity of circular CFT columns, Part I: Theory. Engineering Structures 2008; 30(6): 1573-1578.

[28] Liang Q Q, Fragomeni S. Nonlinear analysis of circular concrete-filled steel tubular short columns under axial loading. Journal of Constructional Steel Research 2009; 65(12): 2186-2196.

[29] Liang QQ, Fragomeni S. Nonlinear analysis of circular concrete-filled steel tubular short columns under eccentric loading. Journal of Constructional Steel Research 2010; 66(2): 159-169.

[30] Choi KK, Xiao Y. Analytical studies of concrete-filled circular steel tubes under axial compression. Journal of Structural Engineering, ASCE 2010; 136 (5): 565-573.

[31] Liang QQ. High strength circular concrete-filled steel tubular slender beam-columns, Part I: Numerical analysis. Journal of Constructional Steel Research 2011; 67(2): 164-171.

[32] Liang QQ. High strength circular concrete-filled steel tubular slender beam-columns, Part II: Fundamental behavior. Journal of Constructional Steel Research 2011; 67(2): 172-180.

[33] Portolés JM, Romero ML, Filippou FC, Bonet JL. Simulation and design recommendations of eccentrically loaded slender concrete-filled tubular columns. Engineering Structures 2011; 33(5): 1576-1593.

[34] Hassanein, MF, Kharoob OF, Liang QQ. Behaviour of circular concrete-filled lean duplex stainless steel-carbon steel tubular short columns. Eng Struct 2013;56:83-94.

[35] Chacón R, Mirambell E, Real E. Strength and ductility of concrete-filled tubular piers of integral bridges. Engineering Structures 2013; 46: 234-246.

[36] Mollazadeh MH, Wang YC. New insights into the mechanism of load introduction into concrete-filled steel tubular column through shear connection. Eng Struct 2014;75 :139–151.

[37] Kostic SM, Filippou FC, Deretic-Stojanovic B. Generalized plasticity model for inelastic RCFT column response. Computers and Structures 2016; 168: 56-67.

[38] Wei S, Mau ST, Vipulanandan C, Mantrala SK. Performance of new sandwich tube under axial loading: Analysis. Journal of Structural Engineering, ASCE 1995; 121(12): 1815-1821.

[39] Huang H, Han LH, Tao Z, Zhao XL. Analytical behavior of concrete-filled double skin steel tubular (CFDST) stub columns. Journal of Constructional Steel Research 2010; 66: 542-555.

[40] Hu HT, Su FC. Nonlinear analysis of short concrete-filled double skin tube columns subjected to axial compressive forces. Marine Structures 2011; 24: 319-337.

[41] Pagoulatou M, Sheehan T, Dai XH, Lam D. Finite element analysis on the capacity of circular concrete-filled double-skin steel tubular (CFDST) stub columns. Engineering Structures 2014; 72: 102-112.

[42] Han HL, Yao GH, Tao Z. Performance of concrete-filled thin-walled steel tubes under pure torsion. Thin-Walled Structures 2007; 45(1): 24-36.

[43] Liang QQ. Performance-based analysis of concrete-filled steel tubular beam-columns. Part I: Theory and algorithms. Journal of Constructional Steel Research 2009; 65(2): 363-373.

[44] Liang QQ. Performance-based analysis of concrete-filled steel tubular beam-columns. Part II: Verification and applications. Journal of Constructional Steel Research 2009; 65(2): 351-362.

[45] Liang QQ. Analysis and design of steel and composite structures. Boca Raton and London: CRC Press, Taylor and Francis Group; 2014.

[46] Patel VI, Liang QQ, Hadi, MNS. Nonlinear analysis of concrete-filled steel tubular columns. Scholar's Press: Germany; 2015.

[47] Mander JB, Priestly MNJ, Park R. Theoretical stress-strain model for confined concrete. Journal of Structural Engineering, ASCE 1988; 114(8):1804-1826.

[48] ACI-318. Building Code Requirements for Reinforced Concrete. ACI, Detroit, MI, 2011.

[49] Richart FE, Brandtzaeg A, Brown RL. A study of the failure of concrete under combined compressive stresses. Bull. 185, University of Illinois, Engineering experimental Station, Champaign, III, 1928.

[50] Park R. (1989). Evaluation of ductility of structures and structural subassemblages from laboratory testing. Bull. of the New Zealand Soc. for Earthquake Engrg., 22(3): 155–166.

Figures and Tables

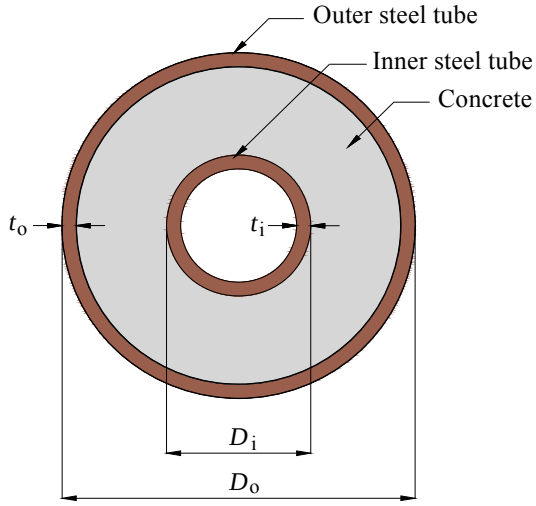

Fig. 1. Cross-section of circular DCFST column

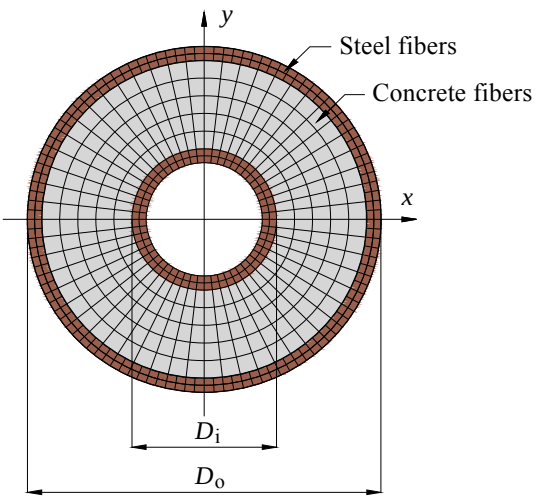

Fig. 2. Typical fiber element discretization of circular DCFST column.

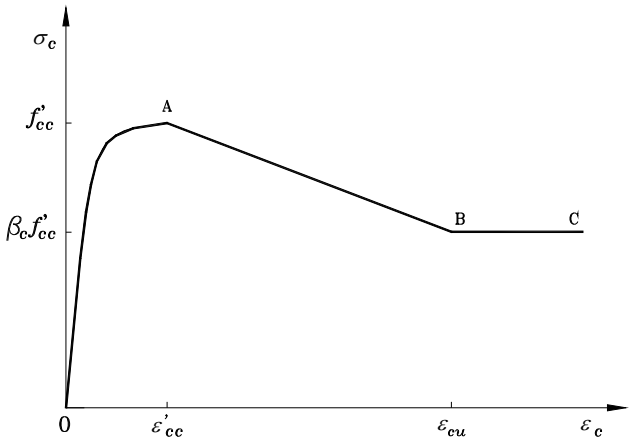

Fig. 3. Stress-strain curve for sandwiched concrete in circular DCFST columns

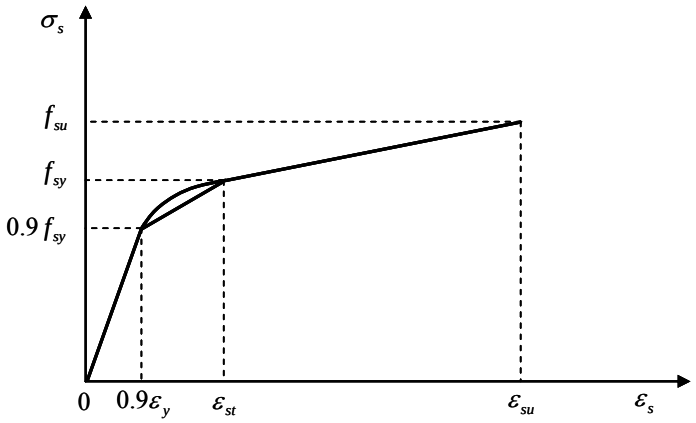

Fig. 4. Stress-strain curve for structural steels

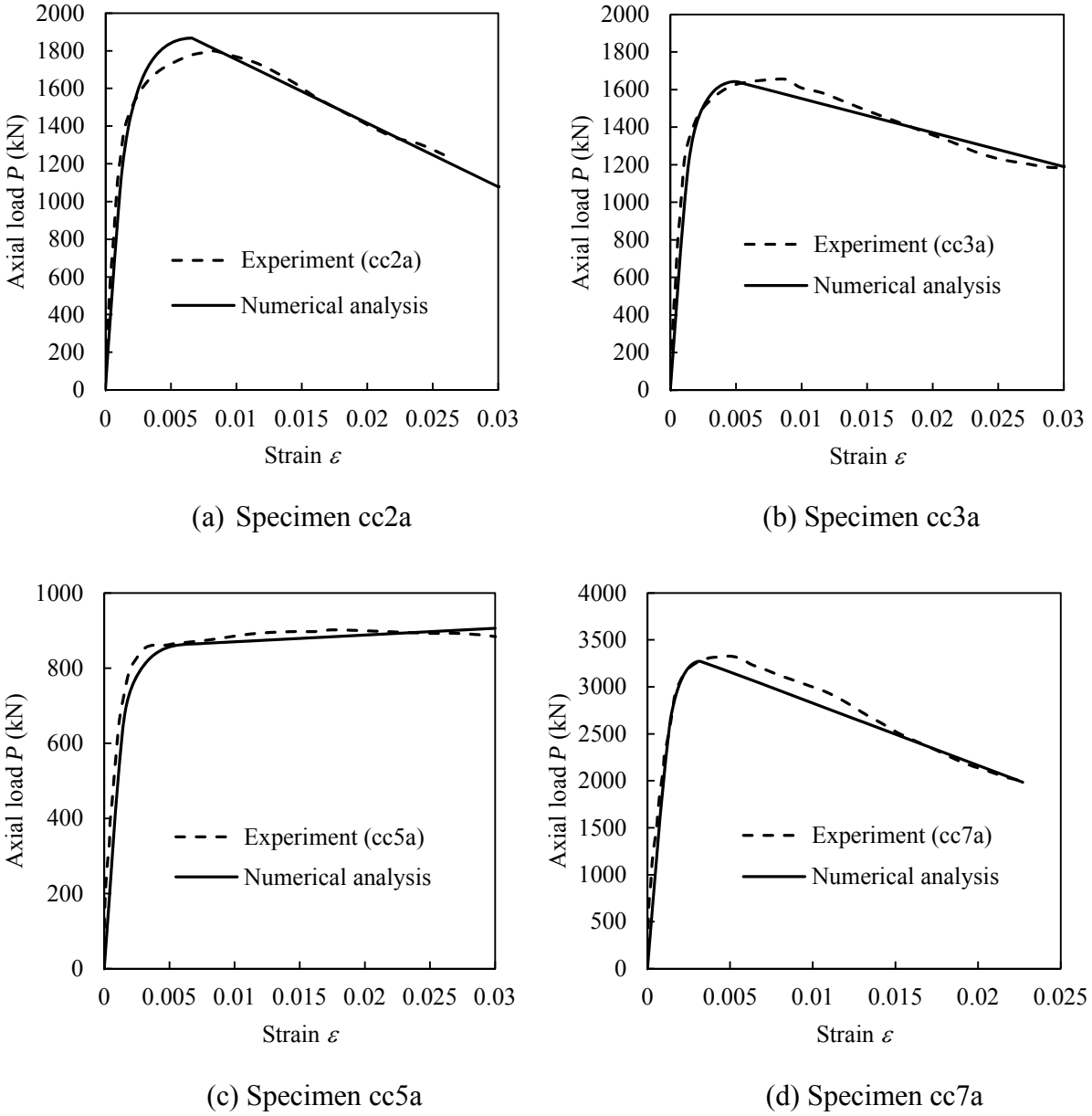

(a) Specimen cc2a

(b) Specimen cc3a

(c) Specimen cc5a

(d) Specimen cc7a

Fig. 5. Comparison of predicted and experimental axial load-strain curves for circular DCFST short columns

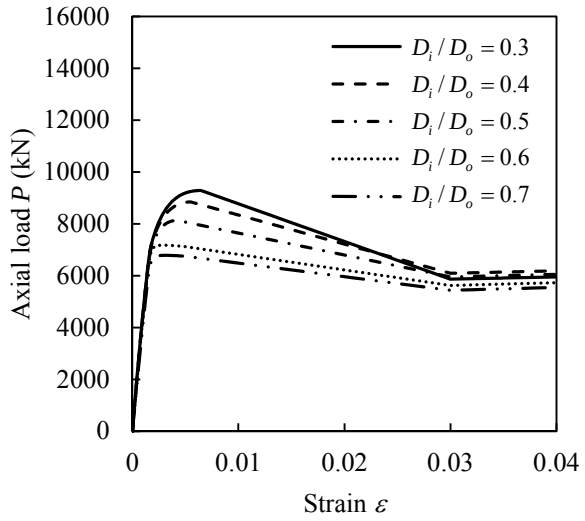

Fig. 6. Axial load-strain curves for DCFST short columns with various D_i / D_o ratios

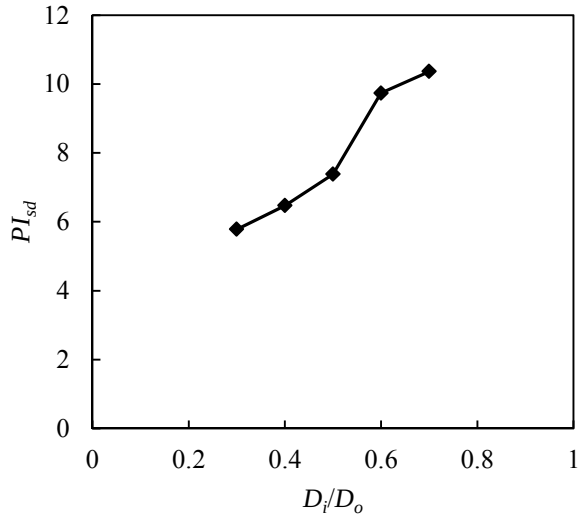

Fig. 7. Strain ductility indices of DCFST short columns with various D_i / D_o ratios

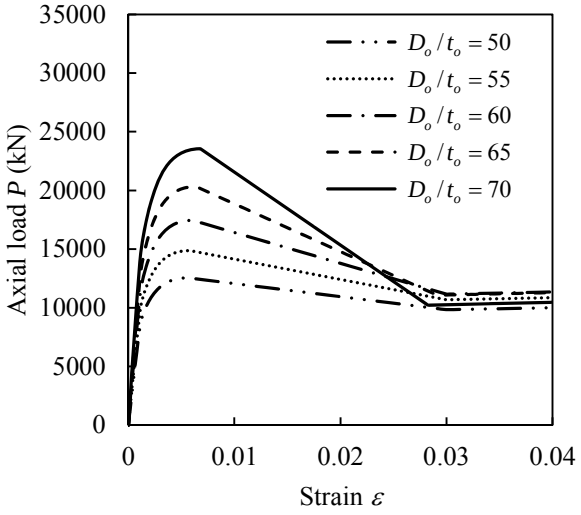

Fig. 8. Axial load-strain curves for DCFST short columns with various D_o/t_o ratios ($D_o = 500, 550, 600, 650, 700$ mm, $t_o = 10$ mm)

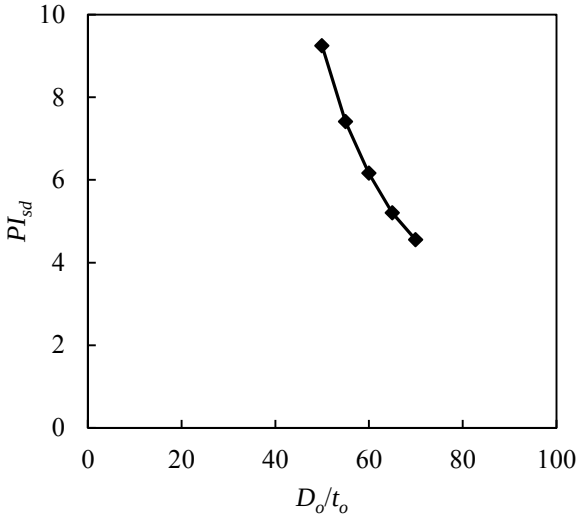

Fig. 9. Strain ductility indices of DCFST short columns with various D_o/t_o ratios ($D_o = 500, 550, 600, 650, 700$ mm, $t_o = 10$ mm)

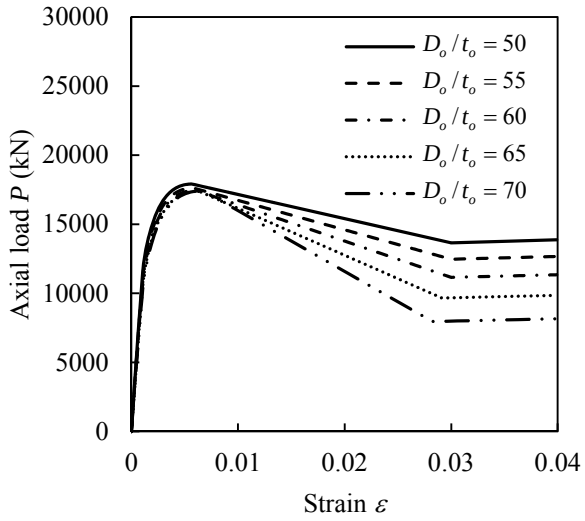

Fig. 10. Axial load-strain curves for DCFST short columns with various D_o/t_o ratios ($D_o = 600\,\text{mm}, t_o = 12, 10.91, 10, 9.23, 8.57\,\text{mm}$)

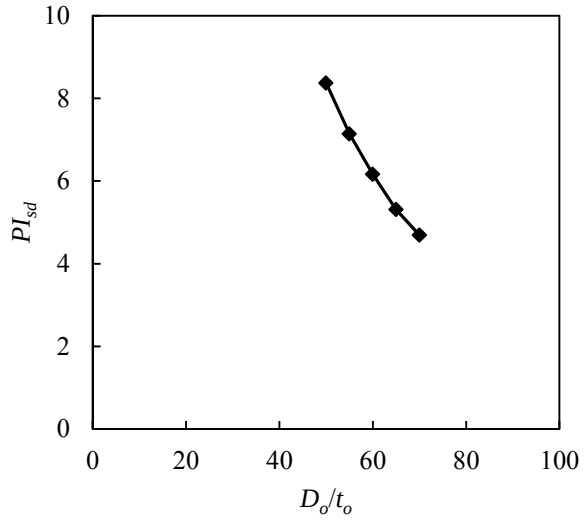

Fig. 11. Strain ductility indices of DCFST short columns with various D_o/t_o ratios ($D_o = 600\,\text{mm}, t_o = 12, 10.91, 10, 9.23, 8.57\,\text{mm}$)

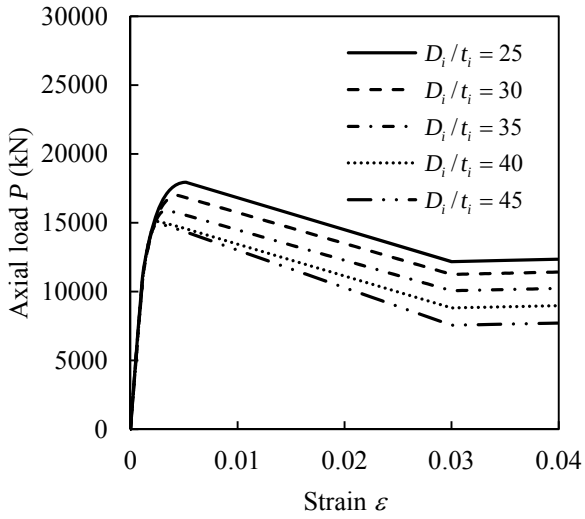

Fig. 12. Axial load-strain curves for DCFST short columns with various D_i/t_i ratios

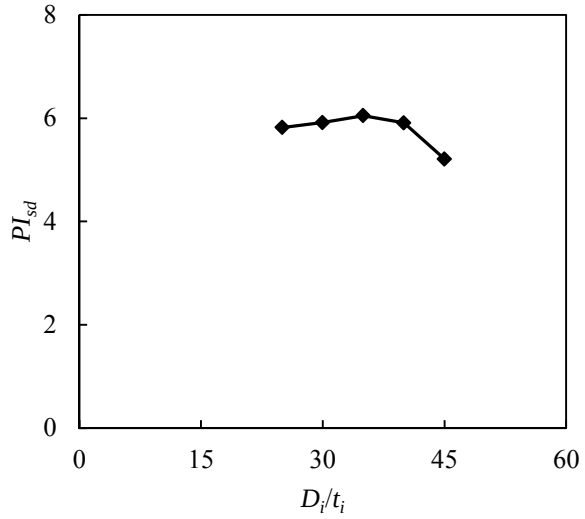

Fig. 13. Strain ductility indices of DCFST short columns with various D_i/t_i ratios

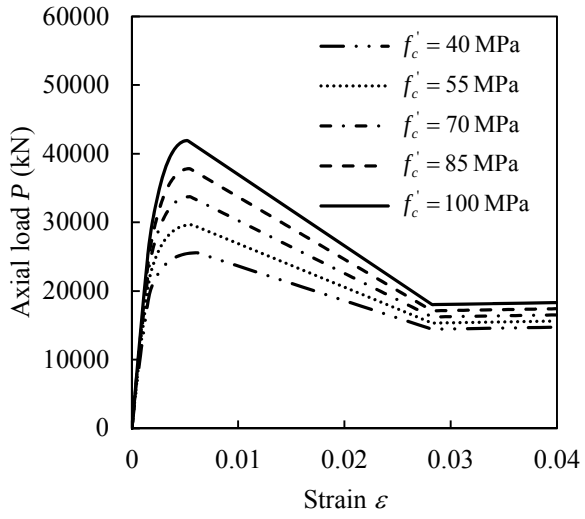

Fig. 14. Axial load-strain curves for DCFST short columns made of different strength concrete

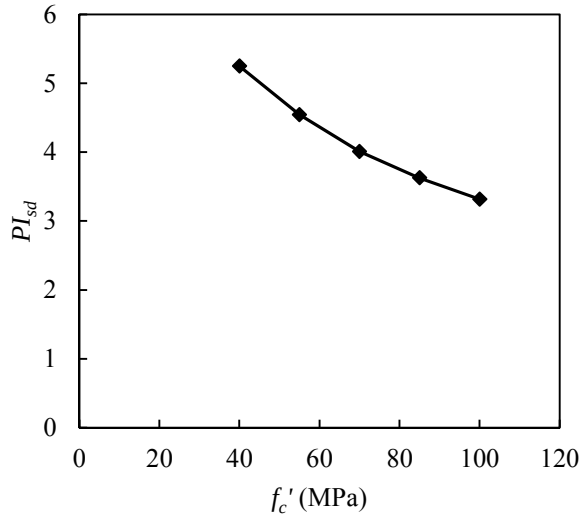

Fig. 15. Strain ductility indices of DCFST short columns made of different strength concrete

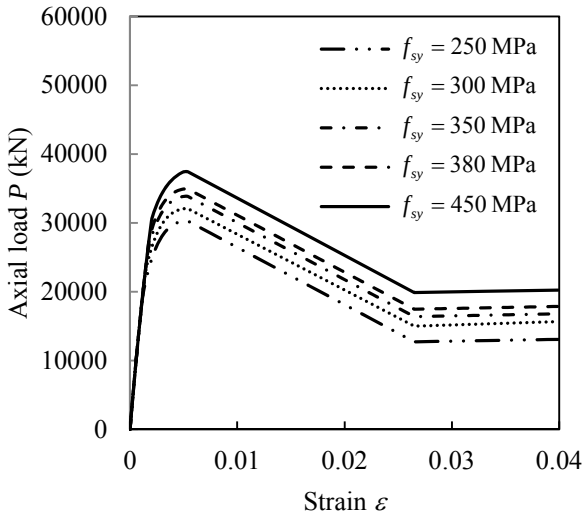

Fig. 16. Axial load-strain curves for DCFST short columns made of different strength steel tubes

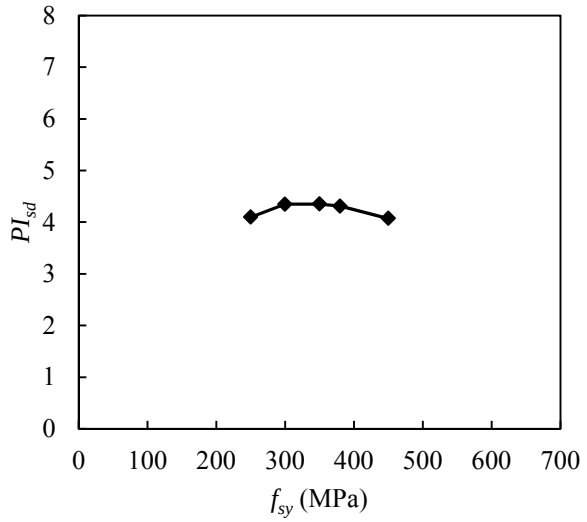

Fig. 17. Strain ductility indices of DCFST short columns made of different strength steel tubes

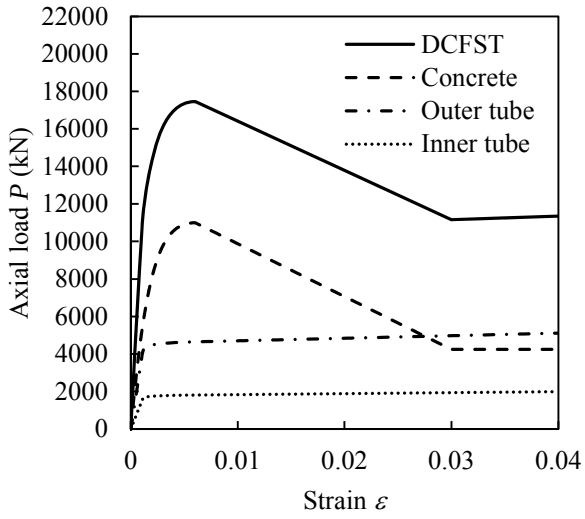

Fig. 18. Axial loads carried by the steel and concrete components and DCFST column

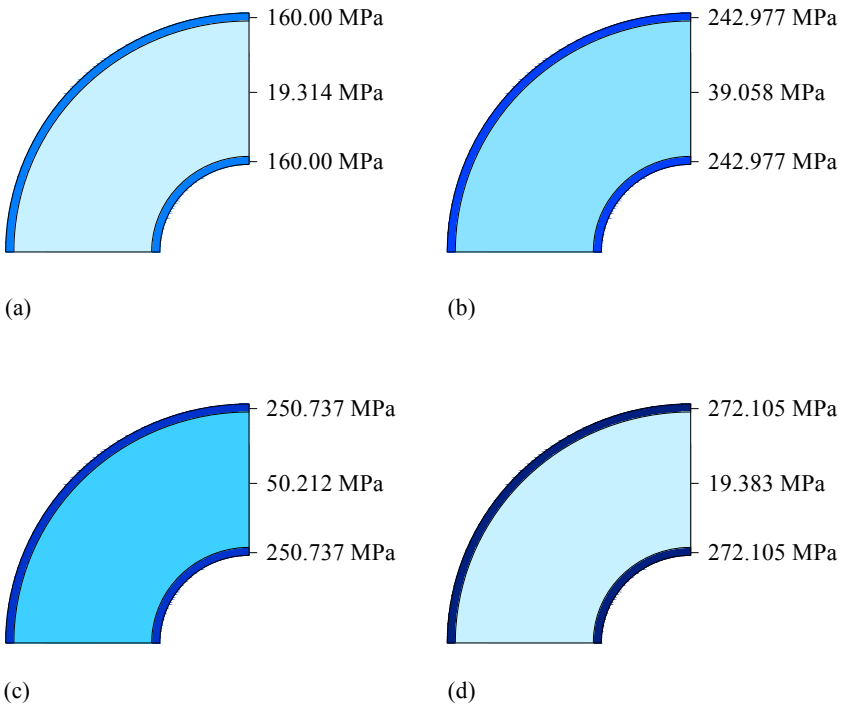

Fig. 19. Distribution of longitudinal stresses in steel and concrete of DCFST column at different axial strain levels: (a) $\varepsilon = 0.0008$; (b) $\varepsilon = 0.0022$; (c) $\varepsilon = 0.006$; (d) $\varepsilon = 0.035$

Table 1. Strength degradation parameter k_3 for sandwiched concrete

D_o/t_o	D_i/t_i	k_3	D_o/t_o	D_i/t_i	k_3	D_o/t_o	D_i/t_i	k_3
45	15	0.687	65	15	0.124	85	15	-0.726
45	20	0.650	65	20	0.222	85	20	-0.495
45	25	0.585	65	25	0.290	85	25	-0.292
45	30	0.490	65	30	0.330	85	30	-0.119
45	35	0.366	65	35	0.340	85	35	0.026
45	40	0.214	65	40	0.321	85	40	0.141
45	45	0.032	65	45	0.274	85	45	0.228
45	50	-0.178	65	50	0.197	85	50	0.285
45	55	-0.418	65	55	0.092	85	55	0.313
50	15	0.573	70	15	-0.061	90	15	-0.984
50	20	0.570	70	20	0.070	90	20	-0.719
50	25	0.538	70	25	0.172	90	25	-0.483
50	30	0.477	70	30	0.244	90	30	-0.276
50	35	0.387	70	35	0.288	90	35	-0.098
50	40	0.268	70	40	0.303	90	40	0.051
50	45	0.120	70	45	0.289	90	45	0.171
50	50	-0.057	70	50	0.246	90	50	0.262
50	55	-0.263	70	55	0.174	90	55	0.324
55	15	0.441	75	15	-0.265	95	15	-1.259
55	20	0.472	75	20	-0.101	95	20	-0.961
55	25	0.473	75	25	0.035	95	25	-0.691
55	30	0.446	75	30	0.141	95	30	-0.451
55	35	0.389	75	35	0.219	95	35	-0.240
55	40	0.304	75	40	0.267	95	40	-0.057
55	45	0.189	75	45	0.287	95	45	0.096
55	50	0.046	75	50	0.277	95	50	0.221
55	55	-0.127	75	55	0.239	95	55	0.316
60	15	0.292	80	15	-0.487	100	15	-1.553
60	20	0.356	80	20	-0.289	100	20	-1.221
60	25	0.391	80	25	-0.120	100	25	-0.918
60	30	0.397	80	30	0.020	100	30	-0.644
60	35	0.374	80	35	0.131	100	35	-0.399
60	40	0.322	80	40	0.213	100	40	-0.183
60	45	0.241	80	45	0.266	100	45	0.004
60	50	0.130	80	50	0.290	100	50	0.162
60	55	-0.009	80	55	0.285	100	55	0.291

Table 2. Ultimate axial strengths of circular DCFST short columns

Specimen	$D_o \times t_o$ (mm)	$D_i \times t_i$ (mm)	D_o/t_o	D_i/t_i	f_{yo} (MPa)	f_{yi} (MPa)	f_c' (MPa)	$P_{u.\exp}$ (kN)	$P_{u.\mathrm{num}}$ (kN)	$\frac{P_{u.\mathrm{num}}}{P_{u.\exp}}$	Ref.
cc2a	180×3	48×3	60	16	275.9	396.1	40.3	1790	1867.2	1.043	[17]
cc2b	180×3	48×3	60	16	275.9	396.1	40.3	1791	1867.2	1.043	
cc3a	180×3	88×3	60	29.3	275.9	370.2	40.3	1648	1643.6	0.997	
cc3b	180×3	88×3	60	29.3	275.9	370.2	40.3	1650	1643.6	0.996	
cc4a	180×3	140×3	60	46.7	275.9	342.0	40.3	1435	1216.8	0.848	
cc4b	180×3	140×3	60	46.7	275.9	342.0	40.3	1358	1216.8	0.896	
cc5a	114×3	58×3	38	19.3	294.5	374.5	40.3	904	906	1.002	
cc5b	114×3	58×3	38	19.3	294.5	374.5	40.3	898	906	1.009	
cc6a	240×3	114×3	80	38	275.9	294.5	40.3	2421	2573.9	1.063	
cc6b	240×3	114×3	80	38	275.9	294.5	40.3	2460	2573.9	1.046	
cc7a	300×3	165×3	100	55	275.9	320.5	40.3	3331	3272.3	0.982	
cc7b	300×3	165×3	100	55	275.9	320.5	40.3	3266	3272.3	1.002	
c23-375	158×2.14	40×2.14	73.8	18.7	286	286	18.7	968.2	1020.4	1.054	[18]
c23-750	158×2.14	77×2.14	73.8	36.0	286	286	18.7	879.1	831.5	0.946	
c23-1125	157×2.14	115×2.14	73.4	53.7	286	286	18.7	703.6	650.7	0.925	
Mean										0.990	
Standard deviation (SD)										0.060	
Coefficient of variation (COV)										0.061	

Table 3. Comparison of lateral confining pressure models for sandwiched concrete in circular DCFST short columns

Specimen	$P_{u.\exp}$ (kN)	$f_{rp.1}$ (MPa)	$P_{u.1}$ (kN)	$f_{rp.2}$ (MPa)	$P_{u.2}$ (kN)	$f_{rp.3}$ (MPa)	$P_{u.3}$ (kN)	$\frac{P_{u.1}}{P_{u.\exp}}$	$\frac{P_{u.2}}{P_{u.\exp}}$	$\frac{P_{u.3}}{P_{u.\exp}}$	Ref.
cc2a	1790	3.875	1867.2	12.802	2700.1	9.576	2399	1.043	1.508	1.340	[17]
cc2b	1791	3.875	1867.2	12.802	2700.1	9.576	2399	1.043	1.508	1.339	
cc3a	1648	2.399	1643.6	12.426	2407.8	7.97	2068.2	0.997	1.461	1.255	
cc3b	1650	2.399	1643.6	12.426	2407.8	7.97	2068.2	0.996	1.459	1.253	
cc4a	1435	0.0	1216.8	8.396	1554.6	2.949	1343.1	0.848	1.083	0.936	
cc4b	1358	0.0	1216.8	8.396	1554.6	2.949	1343.1	0.896	1.145	0.989	
cc5a	904	3.6	906	7.334	1005.8	4.72	936	1.002	1.113	1.035	
cc5b	898	3.6	906	7.334	1005.8	4.72	936	1.009	1.120	1.0423	
cc6a	2421	2.441	2573.9	16.245	4510.4	13.709	4154.6	1.063	1.863	1.716	
cc6b	2460	2.441	2573.9	16.245	4510.4	13.709	4154.6	1.046	1.8335	1.689	
cc7a	3331	0.824	3272.3	25.621	8185.9	19.109	6897.6	0.982	2.457	2.071	
cc7b	3266	0.824	3272.3	25.621	8185.9	19.109	6897.6	1.002	2.506	2.112	
c23-375	968.2	4.388	1020.4	13.337	1693.9	14.364	1771.1	1.054	1.750	1.829	[18]
c23-750	879.1	2.175	831.5	13.559	1539.2	11.965	1440.2	0.946	1.751	1.638	
c23-1125	703.6	0.0	650.7	10.032	1040.9	5.721	875	0.925	1.479	1.244	
Mean								0.990	1.602	1.433	
Standard deviation (SD)								0.060	0.427	0.373	
Coefficient of variation (COV)								0.061	0.267	0.260	

Table 4. Geometric and material properties of circular DCFST short columns used in the parametric study

Group	Column	D_o (mm)	t_o (mm)	D_o/t_o	D_i (mm)	t_i (mm)	D_i/t_i	f_{syo}, f_{syi} (MPa)	f_{suo}, f_{sui} (MPa)	f_c' (MPa)	f_{rp} (MPa)
1	C1	400	6.67	60	120	6	20	350	430	40	3.637
	C2	400	6.67	60	160	6	26.7	350	430	40	2.849
	C3	400	6.67	60	200	6	33.3	350	430	40	1.573
	C4	400	6.67	60	240	6	40	350	430	40	0.000
	C5	400	6.67	60	280	6	46.7	350	430	40	0.000
2	C6	500	10	50	240	10	24	250	320	40	2.918
	C7	550	10	55	240	10	24	250	320	40	3.040
	C8	600	10	60	240	10	24	250	320	40	3.224
	C9	650	10	65	240	10	24	250	320	40	3.471
	C10	700	10	70	240	10	24	250	320	40	3.780
3	C11	600	12	50	240	10	24	250	320	40	2.919
	C12	600	10.91	55	240	10	24	250	320	40	3.040
	C13	600	10	60	240	10	24	250	320	40	3.224
	C14	600	9.23	65	240	10	24	250	320	40	3.471
	C15	600	8.57	70	240	10	24	250	320	40	3.780
4	C16	550	10	55	250	10	25	250	320	60	2.897
	C17	550	10	55	250	8.33	30	250	320	60	2.014
	C18	550	10	55	250	7.14	35	250	320	60	0.857
	C19	550	10	55	250	6.25	40	250	320	60	0.000
	C20	550	10	55	250	5.56	45	250	320	60	0.000
5	C21	700	10	70	280	10	28	350	430	40	3.288
	C22	700	10	70	280	10	28	350	430	55	3.288
	C23	700	10	70	280	10	28	350	430	70	3.288
	C24	700	10	70	280	10	28	350	430	85	3.288
	C25	700	10	70	280	10	28	350	430	100	3.288
6	C26	800	10	80	360	10	36	250	320	50	2.879
	C27	800	10	80	360	10	36	300	430	50	2.879
	C28	800	10	80	360	10	36	350	430	50	2.879
	C29	800	10	80	360	10	36	380	460	50	2.879
	C30	800	10	80	360	10	36	450	520	50	2.879

Table 5. Comparisons of calculated and experimental ultimate axial loads of circular DCFST short columns

Specimen	γ_c	f_c' (MPa)	f_{rp} (MPa)	γ_{so}	γ_{si}	f_{sy0} (MPa)	f_{syi} (MPa)	$P_{u.\mathrm{cal}}$ (kN)	$P_{u.\exp}$ (kN)	$\frac{P_{u.\mathrm{cal}}}{P_{u.\exp}}$
cc2a	1.0	40.3	3.875	0.968	1.105	275.9	396.1	1865.5	1790	1.042
cc2b	1.0	40.3	3.875	0.968	1.105	275.9	396.1	1865.5	1791	1.042
cc3a	1.0	40.3	2.405	0.968	1.040	275.9	370.2	1641.6	1648	0.996
cc3b	1.0	40.3	2.405	0.968	1.040	275.9	370.2	1641.6	1650	0.995
cc4a	1.0	40.3	0.0	0.968	0.993	275.9	342.0	1221.9	1435	0.851
cc4b	1.0	40.3	0.0	0.968	0.993	275.9	342.0	1221.9	1358	0.900
cc5a	1.0	40.3	3.604	1.013	1.084	294.5	374.5	881.6	904	0.975
cc5b	1.0	40.3	3.604	1.013	1.085	294.5	374.5	881.6	898	0.981
cc6a	1.0	40.3	2.441	0.941	1.013	275.9	294.5	2542	2421	1.05
cc6b	1.0	40.3	2.441	0.941	1.013	275.9	294.5	2542	2460	1.033
cc7a	1.0	40.3	0.824	0.92	0.977	275.9	320.5	3219.8	3331	0.967
cc7b	1.0	40.3	0.824	0.92	0.977	275.9	320.5	3219.8	3266	0.986
c23-375	1.0	18.7	4.388	0.948	1.088	286	286	998.1	968.2	1.031
c23-750	1.0	18.7	2.175	0.948	1.019	286	286	814.7	879.1	0.927
c23-1125	1.0	18.7	0.0	0.948	0.979	286	286	643.0	703.6	0.914
Mean										0.979
Standard deviation (SD)										0.057
Coefficient of variation (COV)										0.058